Magnetic properties of the $S=\frac{1}{2}$ quasi-one-dimensional antiferromagnet $CaCu_2O_3$

V. Kiryukhin,* Y. J. Kim, K. J. Thomas, and F. C. Chou
Department of Physics, Massachusetts Institute of Technology, Cambridge, Massachusetts 02139

R. W. Erwin
NIST Center for Neutron Research, NIST, Gaithersburg, Maryland 20899

Q. Huang
NIST Center for Neutron Research, NIST, Gaithersburg, Maryland 20899
and Department of Materials and Nuclear Engineering, University of Maryland, College Park, Maryland 20742

M. A. Kastner and R. J. Birgeneau†
Department of Physics, Massachusetts Institute of Technology, Cambridge, Massachusetts 02139

We report single-crystal growth and magnetic susceptibility and neutron diffraction studies of the $S=\frac{1}{2}$ quasi-one-dimensional antiferromagnet $CaCu_2O_3$. The structure of this material is similar to that of the prototype two-leg spin-ladder compound $SrCu_2O_3$. However, the Cu-O-Cu bond angle in the ladder rungs in $CaCu_2O_3$ is equal to 123°, and therefore the magnetic interaction along the rung is expected to be much weaker in this material. At high temperatures, the magnetic susceptibility of $CaCu_2O_3$ can be decomposed into a contribution from one-dimensional antiferromagnetic chains or finite-size chain segments together with a weak Curie contribution. The intrachain magnetic exchange constant $J_{\parallel}$, determined from the magnetic susceptibility measurements, is 2000 ± 300 K. $CaCu_2O_3$ undergoes a Néel transition at $T_N = 25$ K with ordering wave vector of $[0.429(5), \frac{1}{2}, \frac{1}{2}]$. The magnetic structure is incommensurate in the direction of the frustrated interchain interaction. Weak commensurate magnetic Bragg peaks with the reduced wave vector $(\frac{1}{2}, \frac{1}{2}, \frac{1}{2})$ are also observed below T_N. Application of a magnetic field induces a metamagnetic transition at which the incommensurability of the magnetic structure is substantially reduced. Above the transition field, the material possesses only short-range magnetic order, and no well defined temperature-driven transition is observed.

I. INTRODUCTION

Low-dimensional quantum spin systems exhibit a variety of intriguing properties originating from the low dimensionality and quantum fluctuations. Quantum effects are most pronounced in $S=\frac{1}{2}$ systems. The one-dimensional (1D) $S=\frac{1}{2}$ nearest-neighbor Heisenberg antiferromagnetic (AF) chain and its two-dimensional (2D) analog, the square lattice antiferromagnet, have been extensively investigated both theoretically and experimentally. The properties of these systems turn out to be very different: the nearest-neighbor Heisenberg AF chain exhibits a critical ground state,[1] while true long-range order takes place at temperature $T=0$ in the 2D system.[2] These observations have motivated extensive research activity that has resulted in the discovery of magnetic systems consisting of a finite number of interacting 1D chains which interpolate between the 1D and 2D cases.

The most notable examples of such systems are planar arrays of strongly coupled n chains, the so-called n-legged spin ladders.[3] $S=\frac{1}{2}$ n-legged spin ladders exhibit fundamentally different properties for even and odd n. Even-legged ladders exhibit a spin liquid ground state with a gap in the magnetic excitation spectrum, while odd-legged ladders exhibit a ground state isomorphous to that of the 1D chain. Several good physical realizations of these systems, notably $Sr_{m-1}Cu_{m+1}O_{2m}$ and $Sr_{14}Cu_{24}O_{41}$, have been found, and the main predictions for the nature of the ground state have been

confirmed experimentally.[3] However, our understanding of these intriguing materials is still incomplete from both the theoretical and experimental points of view.

Adding to the complexity of the picture, frustrated magnetic interactions and disorder are often present in real-life materials and result in new and unexpected phenomena. In the cuprate spin-ladder systems mentioned above, the inter-ladder Heisenberg interactions are indeed essentially frustrated. That is, classically they cancel exactly, and therefore weak magnetic interactions resulting from magnetic anisotropy or from minute lattice distortions should play an important role in these compounds. The effects of frustration and disorder together with the effects of anisotropic interactions on the properties of low-dimensional materials provide a rich field for both theoretical and experimental work. A substantial amount of research activity is currently being devoted to these subjects.

In this paper, we report single crystal growth and magnetic susceptibility and neutron-diffraction studies of the $S=\frac{1}{2}$ quasi-1D magnet $CaCu_2O_3$. The structure of this material, shown in Fig. 1, is similar to that of the prototype two-leg spin-ladder compound $SrCu_2O_3$. It consists of an array of ladderlike structures with quasi-1D copper-oxide chains extending along the crystallographic b direction. However, while the Cu-O-Cu bond angle in the rungs is 180° in the Sr compound,[4] it equals 123° in $CaCu_2O_3$; colloquially, the ladder is ''buckled.'' Therefore, according to the Goodenough-
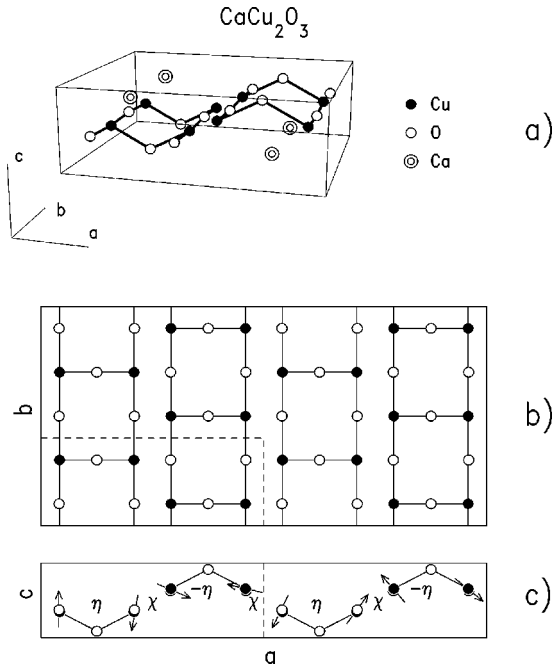
FIG. 1. (a) The atomic structure of $CaCu_2O_3$. (b) The projection on the crystallographic ab plane, and (c) on the ac plane. Ca atoms are not shown. The dotted line indicates the structural unit cell. In (c) arrows correspond to the zero-field model magnetic spiral structure, and η and χ designate the angles between the adjacent spins, as discussed in the text.

Kanamori-Anderson rules,[5] the interchain interaction in the buckled ladders in $CaCu_2O_3$ should be substantially weaker than that in $SrCu_2O_3$. At high temperatures, the temperature-dependent part of the magnetic susceptibility of $CaCu_2O_3$ can be described as the sum of a contribution from one-dimensional antiferromagnetic chains or finite-size chain segments, and a weak Curie contribution. The intrachain magnetic exchange constant $J_\parallel$, determined from the slope of the high-temperature susceptibility curve, is $J_\parallel = 2000 \pm 300$ K. Similar values have been previously reported for the related quasi-1D compounds Sr_2CuO_3 and $SrCuO_2$.[10–12]

$CaCu_2O_3$ undergoes a Néel transition to 3D long-range order at $T_N \sim 25$ K. The magnetic ordering occurs with a three-dimensional-like critical exponent $\beta = 0.3$–0.4. The ordering wave vector is $[0.429(5), \frac{1}{2}, \frac{1}{2}]$. The magnetic structure is incommensurate in the direction of the frustrated interchain interaction. Weak commensurate magnetic Bragg peaks with the reduced wave vector $(\frac{1}{2}, \frac{1}{2}, \frac{1}{2})$ are also observed below T_N. The experimental data are consistent with a spiral (or possibly conical) magnetic structure with spins rotating in the ac crystallographic plane. The low-temperature magnitude of the ordered magnetic moment determined using this model magnetic structure is $0.2 \pm 0.07 \mu_B$. The observed incommensurate magnetic structure can result either from the presence of anisotropic magnetic interactions, or from the existence of a lattice distortion lifting the frustration of the interladder Heisenberg interaction. It is also possible that transverse incommensurate magnetic correlations are intrinsic to coupled Heisenberg spin ladders and that these correlations are responsible for the observed magnetic structure. The application of a magnetic field induces a metamagnetic transition in which the incommensurability of the magnetic structure is substantially reduced. The material possesses only short-range magnetic order above the transition field.

The format of this paper is as follows. In Sec. II, we describe the single-crystal growth and the sample characterization, together with experimental details of the magnetic susceptibility and neutron-diffraction measurements. Section III presents the results and analysis of the magnetic susceptibility measurements. In Sec. IV, we discuss neutron-diffraction measurements of the crystal structure, zero-field magnetic ordering, and also the effects of a magnetic field. Finally, in Sec. V we give a summary and conclusions.

II. EXPERIMENTAL DETAILS

$CaCu_2O_3$ has an orthorhombic lattice, space group $Pmmn$,[6] with $a = 9.949$ Å, $b = 4.078$ Å and $c = 3.460$ Å at $T = 10$ K. Single crystals of $CaCu_2O_3$ have been grown using the traveling solvent floating zone (TSFZ) method with CuO as a flux. To prepare $CaCu_2O_3$ powder, a mixture of $CaCO_3$ and CuO powders was calcined at 850 °C for 12 h with subsequent heating at 995 °C in air for 3 days with frequent grindings. Only small amounts of Ca_2CuO_3 and CuO impurities have been found in the as-prepared powder. Oxygen or inert gas annealing at 995 °C does not result in any significant magnetic or structural change, which implies that the oxygen content is close to being stoichiometric.

The growth is carried out in a four-lamp optical FZ furnace built by Crystal Systems Inc. The temperature range, in which crystals of the required composition are stable, 975–1020 °C, is extremely narrow,[7] requiring careful temperature control. We use as-prepared powder to make feed rods. To reduce the radial thermal gradient of the hot zone, feed rods with diameter less than 5 mm are used. By careful observation of the amount of extra feed rod that dissolves into the molten zone, we estimate that 17.8% CaO/82.2% CuO is the optimal initial concentration of the flux rod. Stable growth is achieved using a pulling rate of 0.8 mm/h, a 35-rpm rotation rate, and an ambient gas flow of oxygen (220 ml/min) and argon (20 ml/min). The growth direction in the obtained crystals is approximately parallel to the copper-oxide chain (010) direction.

Magnetic susceptibility measurements in the temperature interval 2–800 K were carried out using a commercial Quantum Design superconducting quantum interference device magnetometer equipped with a furnace attachment. To perform measurements with the magnetic field oriented along chosen crystallographic axes, the crystals were aligned using x-ray-diffraction techniques.

For single-crystal neutron diffraction experiments, two single grain crystals of $CaCu_2O_3$ with mosaicities of $\sim 0.2°$ from two different batches were chosen. We refer to them as sample 1 and sample 2. The samples were of cylindrical shape, ~ 4 mm in diameter and ~ 20 mm in height. Neutron powder-diffraction measurements performed on powder samples prepared from various other single crystals showed that up to 7% by weight of the impurity phase Ca_2CuO_3 may
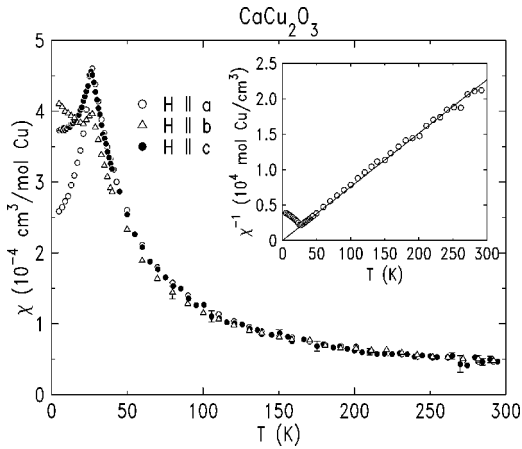
FIG. 2. Temperature dependence of the magnetic susceptibility of $CaCu_2O_3$ in a magnetic field of 1 kG oriented along the three major crystallographic axes, with the temperature-independent part subtracted. The inset shows the inverse magnetic susceptibility after subtracting the T-independent part. The solid line is the result of a fit to the Curie form.

be present. However, no single-crystalline phase other than $CaCu_2O_3$ was detected in the investigated samples. Therefore any impurity phase, if present, was in the form of scattered powder inclusions.

The neutron-diffraction measurements were carried out at the reactor of the National Institute of Standards and Technology (NIST). The powder-diffraction experiment was carried out at the BT-1 high-resolution powder diffractometer. The data were collected in the 2θ range $3-165°$ using a neutron beam of wavelength 1.5401 Å produced by a copper (311) monochromator. The collimations used were $15'-20'-S-7'$. Data were collected at 295, 40, and 10 K. Crystal structure refinements were carried out using the GSAS program.[8] Single-crystal measurements were performed at the BT-2 and BT-9 triple axis spectrometers, using neutrons of energy 14.7 and 30.5 meV for the measurements with and without applied magnetic field, respectively. Pyrolytic graphite (002) monochromator and analyzer crystals were used. To reduce higher energy harmonics present in the beam, pyrolytic graphite filters were placed before and after the sample. The collimations used were $60'-60'-S-80'-80'$ and $60'-40'-S-40'-40'$ for the measurements taken in zero and applied magnetic field, respectively. Zero-field experiments were performed using either a closed cycle helium refrigerator with base temperature 10 K, or a pumped helium cryostat which allowed one to perform measurements down to $T=1.5$ K. Data were taken in the (h,k,k), $(h,k,3k)$, $(h,3k,k)$, and $(h,5k,k)$ scattering planes. A 9-T vertical field superconducting magnet was used for the measurements in an applied field, and the experiment in a field was performed in the $(h,3k,k)$ scattering plane.

III. TEMPERATURE-DEPENDENT SUSCEPTIBILITY

Figure 2 shows the temperature dependence of the magnetic susceptibility of $CaCu_2O_3$ for $T<300$ K measured in a magnetic field of 1 kG aligned with the three major crystal-
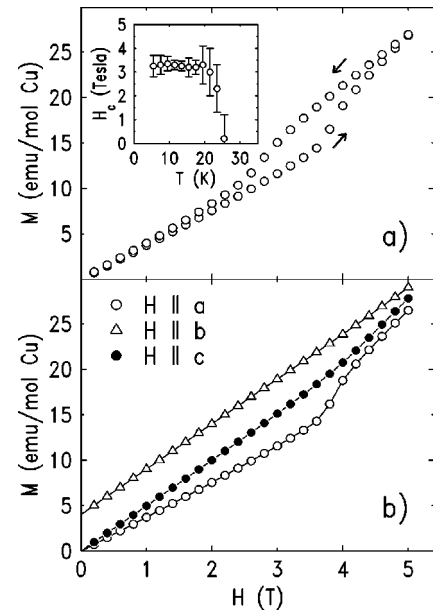

FIG. 3. (a) Magnetization versus magnetic field for $H\|a$ on ramping the field up and down. (b) Magnetization versus magnetic field along the three major crystallographic axes. The temperature is 5 K. The data for the magnetic field aligned with the b axis are shifted up by 4 emu/mol for clarity. The inset shows the temperature dependence of the transition field H_c for the magnetic field parallel to the a axis.

lographic axes. Temperature-independent contributions of 2.23×10^{-4}, 1.73×10^{-4}, and 2.37×10^{-4} cm^3/mol Cu were subtracted from the data of Fig. 2 for the magnetic field aligned with the a, b, and c crystallographic axes, respectively. The sample undergoes a Néel-like transition at T_N ~25 K. The anisotropy of the susceptibility below T_N indicates that spins are mostly confined to the ac crystallographic plane at low temperatures. For temperatures $50<T<300$ K, the temperature dependence of the magnetic susceptibility is well described by Curie $1/T$ behavior (see the inset in Fig. 2). The effective concentration of Cu^{2+} free spins extracted from the corresponding Curie constant amounts to 3% of all the Cu atoms present in the sample. It is impossible, however, to ascribe the Curie term to extraneous impurities since the Curie contribution is dramatically decreased below the Néel temperature, and therefore the ''free'' spins responsible for the Curie term participate in the low-temperature magnetic ordering. Specifically, the data of Fig. 2 imply that the effective concentration of Cu^{2+} free spins present in the sample below $T=25$ K is less than 1%. As shown in Sec. IV, our neutron studies show that at T_N $CaCu_2O_3$ undergoes a transition to a magnetically ordered state with a relatively large value of the ordered magnetic moment, for a quasi-1D $S=\frac{1}{2}$ antiferromagnetic system. This, in turn, means that virtually all of the Cu^{2+} spins participate in the magnetic ordering.

From Fig. 3 one sees that for $T<T_N$ the material undergoes a field induced transition when H is parallel to the crystallographic a axis. The transition results in a small increase of the magnetic moment at $H\sim3$ T at low temperature, and exhibits hysteresis on ramping the magnetic field up and

down for $T < 20$ K. For H parallel to the c axis there is no jump in the moment but the slope of $M(H)$ increases at approximately the same field [see Fig. 3(b)]. The inset in Fig. 3 shows the temperature dependence of the transition field H_c for the magnetic field parallel to the a crystallographic axis. To determine H_c we have averaged the maxima in the field derivative of the magnetization for increasing and decreasing the magnetic field. The error bars in the inset reflect the width of the hysteresis region for $T < 20$ K; at higher temperatures, error bars correspond to the with of the peak in dM/dH. The transition shown in Fig. 3 exhibits some features characteristic of a spin-flop transition in a magnetic system in which spins are confined to the ac crystallographic plane at zero field, but are not parallel to either a or c. In particular, the transition does not occur when the magnetic field is parallel to the b axis. The transition field H_c varies with temperature in the way characteristic to the spin-flop field of a typical anisotropic antiferromagnet.[9] For H parallel to c the transition appears to be continuous even at the lowest temperatures. Such continuous transitions are known to occur in collinear antiferromagnets when the easy axis is not parallel to the applied field,[9] and also in compounds with noncollinear magnetic structures. In Sec. IV we show that the magnetic structure of $CaCu_2O_3$ is, in fact, noncollinear.

The dominant magnetic interaction in $CaCu_2O_3$ is the intrachain coupling $J_\parallel$ which, by analogy to Sr_2CuO_3 and $SrCuO_2$, is expected to be of the order of 2000 K. The spin gap, however, is proportional to the leg coupling $J_\perp$. In $SrCu_2O_3$ $J_\perp \approx \frac{1}{2}J_\parallel$,[11] and the spin gap is equal to 420 K.[13] The approximate value of $J_\perp$ in in $CaCu_2O_3$ can be estimated from the Cu-O-Cu angle in the rungs and from the known values of the magnetic coupling in other copper-oxide based chain compounds. Using the data of Refs. 11 and 14, we obtain $J_\perp \sim 100$–300 K. Because of the reduced value of $J_\perp$ in the buckled ladders of $CaCu_2O_3$, we expect that the material will have a smaller gap than that in $SrCu_2O_3$ and will exhibit 1D behavior characteristic of uncoupled spin-chains above $T \sim 300$–400 K.[15] At lower temperatures, three-dimensional magnetic interactions are, in general, not negligible, and the magnetic susceptibility can only be calculated accurately if these interactions are taken into account. To estimate the numerical value of the intrachain coupling $J_\parallel$, we have used two approaches which are described below.

Figure 4 shows high-temperature susceptibility measured in a field of 1 T approximately aligned with the spin-chain direction. The Curie term is subtracted from these data. The sample starts to decompose at $T \sim 700$ K, and, as a result, the susceptibility abruptly decreases for $T > 700$ K. To analyze the contribution to the magnetic susceptibility from the quasi-1D $S = \frac{1}{2}$ system χ_{spin}, we write χ as

$$\chi = \chi_{Curie} + \chi_{core} + \chi_{vv} + \chi_{spin}, \qquad (1)$$

where χ_{core} is the diamagnetic contribution from the ionic cores, and χ_{vv} is the Van Vleck paramagnetic term. χ_{core} and χ_{vv} are independent of temperature. Equation (1) is phenomenological because, as we have mentioned above, the low-temperature Curie term cannot be ascribed to noninter-
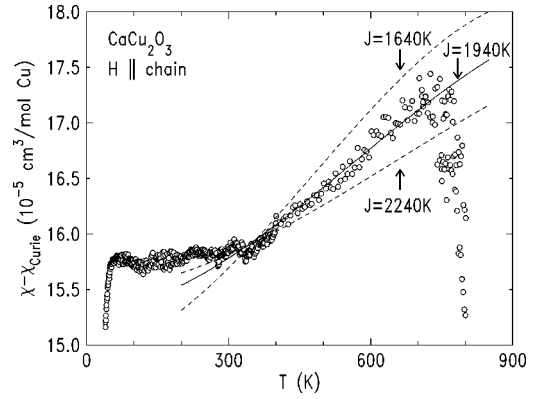

FIG. 4. High-temperature magnetic susceptibility of $CaCu_2O_3$ measured in a magnetic field of 1 T with the Curie part subtracted. The magnetic field points along the crystallographic b axis. The solid and dashed lines are the results of Bethe ansatz calculations for the 1D Heisenberg spin-$\frac{1}{2}$ chain for several values of the intrachain magnetic coupling $J_\parallel$. The sudden drop of the susceptibility above $T = 700$ K is due to sample decomposition.

acting extraneous impurities, and thus, at this stage, Eq. (1) lacks a physical explanation. The high-temperature data of Fig. 4 were fitted to the theoretical results for $\chi(T)$ for a 1D $S = \frac{1}{2}$ chain obtained using the Bethe ansatz method.[16] The solid and dashed curves in Fig. 4 are Bethe ansatz results for three different values of $J_\parallel$ with a temperature-independent term representing $\chi_{core} + \chi_{vv}$ added. Evidently, above $T \sim 300$–400 K and below the sample decomposition temperature, $\chi_{spin}(T)$ is well described by the theoretical curve for a 1D $S = \frac{1}{2}$ chain with $J = 1950 \pm 300$ K. This value is in good agreement with the results for the related quasi-1D chain compounds Sr_2CuO_3, $SrCuO_2$, and $SrCu_2O_3$.[10–12] Using the value $\chi_{core} = -3.3 \times 10^{-5}$ cm^3/mol Cu^{2+} (Ref. 17), we obtain $\chi_{vv} = 1.0 \times 10^{-4}$ cm^3/mol Cu. This result for χ_{vv} is somewhat larger than the previously reported values of $\chi_{vv} = 2$–8×10^{-5} cm^3/mol for Sr_2CuO_3 and $SrCuO_2$.[10] We note that these results are virtually independent of the details of the low-temperature fits that have been used to extract the χ_{Curie} term.

To explain the observed temperature-dependent magnetic susceptibility at a microscopic level, we consider a model in which impurities or structural imperfections break the quasi-1D magnetic chains into weakly interacting segments of finite size. We have calculated the susceptibility of finite spin-chain segments using quantum Monte Carlo simulations utilizing the loop cluster algorithm.[18,19] The only parameters in these calculations are the size of the chain segments, and the intrachain magnetic coupling $J_\parallel$. We use $g = 2.1$ for the Landé factor, which is a typical value for Cu^{2+} in insulator cuprate compounds.[11] Chain segments with even and odd number of spins exhibit qualitatively different behavior. In our calculations, we assume that identical numbers of "even" and "odd" segments are present. We find that this model reproduces the Curie-like behavior of the magnetic susceptibility at low temperatures, as well as the gradual increase of the susceptibility with temperature at high temperatures. However, to achieve satisfactory agreement with the experimental data, it is necessary to add a small additional
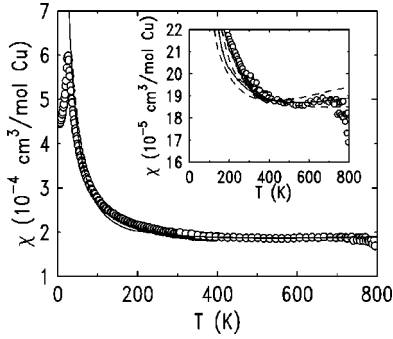
FIG. 5. High-temperature magnetic susceptibility of $CaCu_2O_3$ measured in a magnetic field of 1 T aligned with the spin-chain (b) direction. The solid line is the result of a Monte Carlo calculation for the finite-segment model described in the text with $J_{\parallel}=1940$ K. The inset shows the high-temperature magnetic susceptibility on an expanded scale. The dashed lines are the results of Monte Carlo calculations with $J_{\parallel}=1500$ K and $J_{\parallel}=2500$ K. The sudden drop of the susceptibility above $T=700$ K is due to sample decomposition.

Curie term to the calculated susceptibility. The magnetic susceptibility in this model is therefore given by the same equation as the phenomenological model discussed above [Eq. (1)] in which χ_{spin} now stands for the magnetic susceptibility of the finite 1D chain segments.

In Fig. 5 we show the $CaCu_2O_3$ magnetic susceptibility data together with the results of Monte Carlo calculations for the susceptibility of equal numbers of spin chains consisting of segments with 13 or 14 spins in every segment. We use $J_{\parallel}=1940$ K for the intrachain exchange. A Curie term corresponding to a 1% effective concentration of Cu^{2+} free spins, as well as Van Vleck $\chi_{vv}=9.4\times10^{-5}$ cm^3/mol Cu and ionic core $\chi_{core}=-3.3\times10^{-5}$ cm^3/mol Cu contributions are added. Calculations for the finite-segment model with segments containing more than 20 spins, or less than 10 spins, are incompatible with the experimental data. Thus, in the context of this model, a substantial number of weak links in the magnetic chains is required to explain the observed magnetic susceptibility. Such weak links can occur due to presence of oxygen vacancies or extrinsic impurities. Whether or not the actual concentration of defects in the crystal structure of our samples can explain the large number of weak links required by the finite-segment model will be the subject of future work.

The results of our calculations exhibit systematic deviations from the experimental data for temperatures below $T=300$ K. This indicates that, as expected, interchain interactions are not negligible at these temperatures. However, our Monte Carlo calculations, that were carried out in absolute units with a small number of adjustable parameters for a simple finite-segment model, are clearly in good qualitative agreement with the experimental data. Therefore we believe that the finite-segment model provides a plausible explanation for the unusual temperature dependence of the magnetic susceptibility, including the presence of the Curie-like term at temperatures higher than T_N. Since all of the copper spins are expected to participate in the low-temperature 3D magnetic ordering, this term should disappear below the Néel temperature, in agreement with the experimental results.

TABLE I. Atomic coordinates and temperature parameters for $CaCu_2O_3$ at $T=10$ K. The space group is $Pmmn$. The lattice parameters are $a=9.9491(1)$ Å, $b=4.0775(1)$ Å, $c=3.4604(1)$ Å. The atomic positions are given in the lattice parameter units. The temperature parameters B for the oxygen atoms were constrained to be equal in the refinement.

Atom	x	y	z	B (Å^2)
Ca	0.25	0.25	0.3630(5)	0.71(2)
Cu	0.0829(1)	0.75	0.8436(3)	0.64(2)
O(1)	0.25	0.75	0.5832(4)	0.94(2)
O(2)	0.0812(1)	0.25	0.8720(4)	0.94(2)

At temperatures higher than $T=300$ K, the agreement of the finite-segment model with the experimental data is satisfactory (see the inset in Fig. 5). The value of the intrachain coupling $J_{\parallel}=2000\pm500$ K extracted from the high-temperature fits to this model is insensitive to both the size of the chain segments and to the magnitude of the added Curie term. Therefore the two models described above give the same value of $J_{\parallel}$ within the errors.

IV. NEUTRON DIFFRACTION

A. Zero-field measurements

The structure of $CaCu_2O_3$ is shown in Fig. 1. The corresponding atomic coordinates and temperature parameters determined in the neutron powder-diffraction experiment at $T=10$ K ($R_p=3.53\%$, $R_{wp}=4.45\%$) are listed in Table I. The structure contains copper oxide chains running along the crystallographic b direction; the chains form ladderlike pairs as shown in Fig. 1. As we have mentioned above, the main structural difference between $CaCu_2O_3$ and its Sr analog is that in $CaCu_2O_3$ the Cu-O-Cu angle in the rungs of the ladders is 123°, while the corresponding angle equals 180° in $SrCu_2O_3$. As in $SrCu_2O_3$, the ladders are coupled to each other via $\sim90°$ Cu-O-Cu bonds in the a direction. In the crystallographic c direction, the copper oxide ladders are stacked on top of each other with Ca atoms in between.

$CaCu_2O_3$ undergoes a 3D Néel transition at $T_N\sim25$ K. Figure 6 shows an elastic neutron-diffraction scan along the (h, 0.5, 0.5) direction at $T=12$ K. (The wave-vector transfers are quoted in reciprocal lattice units, r.l.u.) Below $T=25$ K, superlattice Bragg peaks with reduced wave vector [0.429(5), 0.5, 0.5] are detected. Note that, within the accuracy of our experiment, these peaks can be described as commensurate peaks at the (3/7, 0.5, 0.5) position. In this case, the magnetic unit cell is seven times larger than the chemical unit cell in the crystallographic a direction. Much weaker scattering is also found at the (0.5, 0.5, 0.5) positions. The latter peaks are not due to nuclear multiple-scattering effects since they are temperature dependent and disappear above T_N (see Fig. 7). The intensity ratio of the (0.5, 0.5, 0.5) peak to the (0.429, 0.5, 0.5) peak is sample dependent, and specifically, in sample 2 this ratio is approximately two times smaller than that in sample 1.

The data of Fig. 6 and the corresponding data taken at various temperatures have been fitted to three resolution-
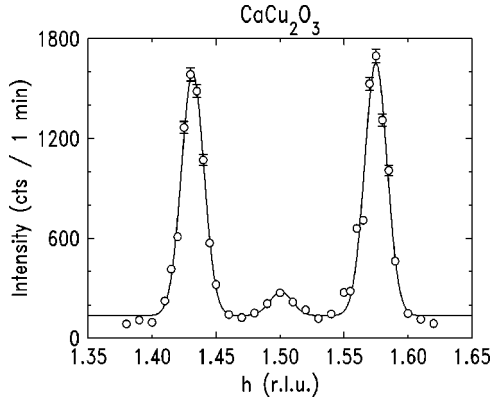
FIG. 6. Neutron-diffraction scan along the $(h, 0.5, 0.5)$ direction at $T = 12$ K in sample 1. The solid line is the result of a fit to three resolution-limited Gaussian peaks as described in the text.

limited Gaussian peaks. The position of the central peak was fixed at the commensurate value of (1.5, 0.5, 0.5). The temperature dependence of the magnetic Bragg peak intensities is shown in Fig. 7. The critical exponent β and the Néel temperature T_N are extracted by fitting the data to the power law $I \sim (1 - T/T_N)^{2\beta}$. For samples 1 and 2 the parameters are found to be $T_N = 25.7(0.2)$, 25.4(0.2), $\beta = 0.35(0.03)$, and 0.44(0.04), respectively. The large values of β indicate that the transition has a three-dimensional Heisenberg character. The differences between the samples are likely due to slight variations in their composition. Despite these differences, the positions of the incommensurate peaks are the same in the both samples. The positions of these peaks are temperature independent.

Neutron-diffraction data were also collected in the $(h, k, 3k)$, $(h, 3k, k)$, and $(h, 5k, k)$ reciprocal space zones. Altogether, the integrated intensities for 27 magnetic Bragg reflections were measured at $T = 12$ K. These data were used for the determination of the low-temperature magnetic structure described in the next section.
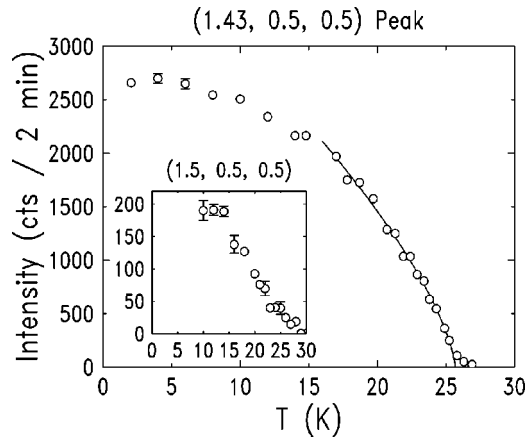

FIG. 7. The intensity of the (1.429, 0.5, 0.5) magnetic peak as a function of temperature in sample 1. The solid line is the result of a fit to a power law as described in the text. The inset shows the temperature dependence of the intensity of the (1.5, 0.5, 0.5) commensurate magnetic peak.

B. Zero-field magnetic structure

In this section we present a simple model magnetic structure consistent with our experimental observations. To construct a plausible model, we first consider the magnetic interactions known to be present in $CaCu_2O_3$. The magnetic interaction is strongest along the copper-oxide chains. As shown in Sec. III, the intrachain Heisenberg exchange constant is $J_\parallel = 2000 \pm 300$ K. The rung exchange constant $J_\perp$ is greatly reduced compared to $J_\parallel$ because of the reduced Cu-O-Cu angle in the rungs. Due to the diminished rung coupling, the energy gained upon the transition to the gapped spin liquid state is also diminished since this gain is proportional to the gap value, which goes to zero in the limit of decoupled chains.[3] Therefore the three-dimensional magnetic interactions in $CaCu_2O_3$ are relatively more important than those in $SrCu_2O_3$. The fact that the former compound undergoes a 3D Néel transition at $T_N = 25$ K while the latter stays in the nonmagnetic state down to the lowest temperatures[13] is consistent with this suggestion.

However, since the Cu-O-Cu angle is different from 180°, in addition to the Heisenberg coupling a Dzyaloshinsky-Moriya (DM) interaction is also present in the rungs of the ladder. This interaction is of the form[20] $H_{DM} = \mathbf{D} \cdot \mathbf{S}_i \times \mathbf{S}_j$. The magnitude of the DM vector D can be estimated[21] as $D \sim (\Delta g/g) J_\perp \Phi$, where Δg is the shift of the gyromagnetic ratio g from the g value for a free electron, and Φ is the deviation of the Cu-O-Cu rung angle from 180°. Since $\Delta g/g$ is typically of the order of 0.1, $\Phi \sim 1$, and our rough estimate for $J_\perp$ is 10–30 meV, D may be as large as several meV. The direction of the DM vector is defined by the lattice symmetry.[22] In $CaCu_2O_3$, it points along the b axis; the DM vectors for the two ladders belonging to the same chemical unit cell [see Figs. 1(b) and 1(c)] are antiparallel. The DM interaction is anisotropic with the anisotropy energy of the order of $D^2/2J_\perp$. In the present case, it favors configurations with spins confined to the ac plane.

The strongest *interladder* interaction is likely to be along the c axis, in the stacking direction of the ladders. As pointed out by Greven and Birgeneau,[23] the exchange constant along this direction, J_c, should be of the order of 10 meV in $SrCu_2O_3$, and because the geometry is similar, it is likely of the same order of magnitude in $CaCu_2O_3$. The interladder interaction in the a direction is more complex. The Heisenberg interaction in this direction is ferromagnetic and relatively weak ($J_a \sim 10$ meV).[24] Moreover, because of the extremely strong AF *intrachain* interaction $J_\parallel$, the magnetic coupling in the a direction is essentially frustrated. Specifically, in the classical limit the a-direction interladder interaction cancels exactly. Therefore, to a first approximation, the magnetic system consists of an array of 2D double planes in which spins are coupled by Heisenberg interactions with antiferromagnetic coupling constants $J_\parallel$, J_c, and $J_\perp$. In the normal direction (crystallographic a axis), the interplane Heisenberg interaction is frustrated, and the planes are only weakly coupled. A nonzero interplanar magnetic coupling, which is required for the 3D magnetic ordering to occur, can result from weak anisotropic interactions,[24,25] such as the pseudodipolar interaction. Another possibility is that an ap-

propriate lattice deformation, small enough to be undetected in our powder measurements, lifts the exact cancellation of the interladder Heisenberg interaction, thereby providing the necessary interplanar coupling.[26,27] Finally, recent numerical calculations indicate that incommensurate peaks in the static magnetic structure factor can occur in the a-axis direction for certain values of J_a even in the absence of the anisotropic interactions and lattice deformation.[28] These calculations, however, were carried out for the so-called modified trellis lattice which differs in some details from the conventional trellis lattice which appears to be the simplest model lattice describing magnetic interactions in $CaCu_2O_3$. Clearly, further theoretical work is needed to establish which of the possible scenarios discussed above is valid for $CaCu_2O_3$.

In the following refinement, we address the magnetic structure that gives rise to the strong incommensurate reflections; the origin of the weak commensurate peaks will be briefly discussed at the end of this section. Magnetic susceptibility measurements discussed in Sec. III indicate that spins are mostly confined to the ac-crystallographic plane, consistent with the geometry of the DM interaction. Therefore we start with trial structures obeying this restriction and then remove it. Since the unit cell is doubled in the b and c directions, the magnetic structure is of a simple antiferromagnetic type along these axes. At the moment, it is unclear how the interladder interactions give rise to the observed incommensurability along the a axis; a detailed theoretical model is needed to answer this question. In the absence of a detailed theory, we have considered two simple phenomenological models for the incommensurate spin structure: a spin-density wave model, and a spiral model. We have found that the former does not reproduce the experimentally observed magnetic peak intensities. As discussed below, the spiral model is, on the other hand, in reasonable agreement with the experimental data.

In the spiral model [Fig. 1(c)], we assume that the spins rotate by a constant angle χ from ladder to ladder. The net interladder interaction along a is expected to be much weaker than the interaction across the rungs, and therefore the relative orientation of the rung spins is defined by the latter interactions. Since both Heisenberg and DM interactions are present in the rungs, the angle between the rung spins should deviate from 180°. We denote this angle as η. In the classical approximation, $\tan\eta = D/J_\perp \sim (\Delta g/g)\Phi$. The sign of η changes from ladder to ladder together with the direction of the DM vector [see Fig. 1(c)].

At low temperatures, the integrated intensity of the magnetic Bragg peaks is given by[29]

$$I = \frac{AF^2(\mathbf{k})}{\sin(2\theta)} \sum_{\alpha\beta} (\delta_{\alpha\beta} - \hat{k}_\alpha\hat{k}_\beta) \sum_{ll'} \langle S_{l'}^\alpha\rangle\langle S_l^\beta\rangle \exp\{i\mathbf{k}\cdot(l-l')\},$$

(2)

where 2θ is the scattering angle, $\mathbf{k}$ is the scattering vector, l denotes atomic positions, α,β stand for the space indices x, y, and z, and $F(\mathbf{k})$ is the Cu^{2+} magnetic form factor. The sum is taken over all copper atoms in the magnetic unit cell. Since the reduced wave vector of the magnetically ordered state equals, within the accuracy of our experiment, (3/7, 0.5,

TABLE II. Observed integrated (I_{obs}) and calculated intensities (I_{calc}) of incommensurate magnetic Bragg reflections in $CaCu_2O_3$. The measurements were performed at $T=12$ K.

(h, k, l)	I_{obs}	I_{calc}
$(0.43, -0.5, -0.5)$	1770(30)	1674
$(1.43, 0.5, 0.5)$	2030(70)	4010
$(1.43, -0.5, -0.5)$	2330(30)	4010
$(2.43, -0.5, -0.5)$	580(20)	829
$(5.43, -0.5, -0.5)$	162(23)	172
$(0.43, -1.5, -1.5)$	136(12)	201
$(2.43, -1.5, -1.5)$	144(20)	222
$(3.43, -1.5, -1.5)$	150(30)	110
$(4.43, -1.5, -1.5)$	390(110)	357
$(0.43, 0.5, 1.5)$	200(20)	309
$(1.43, 0.5, 1.5)$	1290(60)	1298
$(2.43, 0.5, 1.5)$	225(20)	362
$(3.43, 0.5, 1.5)$	130(23)	168
$(4.43, 0.5, 1.5)$	676(80)	544
$(0.43, 1.5, 0.5)$	746(25)	481
$(-0.43, 1.5, 0.5)$	706(35)	481
$(1.43, 1.5, 0.5)$	1290(175)	1920
$(2.43, 1.5, 0.5)$	363(20)	557
$(3.43, 1.5, 0.5)$	210(50)	191
$(4.43, 1.5, 0.5)$	360(25)	533
$(5.43, 1.5, 0.5)$	70(40)	100
$(0.43, 2.5, 0.5)$	268(15)	104
$(-0.43, 2.5, 0.5)$	270(40)	104
$(1.43, 2.5, 0.5)$	525(15)	414
$(2.43, 1.5, 0.5)$	170(60)	111
$(3.43, 1.5, 0.5)$	110(25)	47
$(4.43, 1.5, 0.5)$	190(20)	138

0.5), we have assumed that the actual magnetic unit cell is $7a\times 2b\times 2c$, expressed in terms of the chemical unit-cell parameters. The anisotropic $3d_{x^2-y^2}$ magnetic form factor was calculated using formulas given in Ref. 30. The period of the lattice modulation fixes χ at $3\pi/7 + \pi n$, where n is an integer.

We use our spiral model spin structure and Eq. (2) to fit the experimental data which consist of 27 magnetic Bragg reflections collected in the (h, k, k), $(h, k, 3k)$, $(h, 3k, k)$, and $(h, 5k, k)$ zones. In addition to η and the spin magnitude S, the tilt of the plane of spin rotation with respect to the crystallographic axes is varied. The best results are achieved for the spins rotating in the ac plane with $\eta = 160° \pm 20°$. The crystallographic reliability index, defined as $R = \Sigma|\sqrt{I_{observed}} - \sqrt{I_{calc}}|/\Sigma\sqrt{I_{observed}}$, is $R = 0.18$ (see Table II). The magnitude of the ordered magnetic moment calculated in this model by comparing the magnetic peak intensities with the intensity of the weak structural Bragg peak $(5,1,1)$ is $0.2 \pm .07\mu_B$.

Despite the relatively large value of R, the simple model described above reproduces the qualitative behavior of the experimental data, such as the high intensity of the peaks with $h = 1.43$ and 4.43 as compared to those with $h = 0.43$, 2.43, and 3.43, together with the growth of the peak intensity

with the projection of the scattering unit vector on the b axis. The value of η is consistent with the rough estimate of the DM constant D given above, and the fitted magnitude of the ordered magnetic moment is typical for quasi-1D $S = \frac{1}{2}$ magnetic systems. Taking into account the simplicity of the model, these results are quite satisfactory. However, our model is in all likelihood oversimplified. It does not, for example, explain the anisotropy of the magnetic susceptibility in the ac plane (see Fig. 2). We have considered elliptic magnetic structures that could account for this anisotropy. Such structures, however, produce fits of similar quality to those obtained using the circular spiral model. Clearly, more theoretical and experimental work is required to elucidate the magnetic structure of $CaCu_2O_3$ in detail.

The weak commensurate scattering at the (0.5, 0.5, 0.5) position can have at least two different origins. Canting of the spins out of the ac plane with canting angle of the order of $10°$ and with the appropriate periodicity is one possible scenario. In this case, a conical magnetic structure is realized. Alternatively, commensurate and incommensurate components can originate from spatially distinct parts of the sample, possibly differentiated by slight compositional variations.

C. Effects of a magnetic field

The application of a magnetic field has a dramatic effect on the low-temperature magnetic structure in $CaCu_2O_3$. According to the magnetic susceptibility measurements of Sec. III, application of a magnetic field along the a or c axis results in a transition at a magnetic field of approximately 3.5 T at low temperatures. Taking into account the zero-field magnetic structure discussed in the previous section, it is natural to expect that, in agreement with the magnetization data of Sec. III, application of a magnetic field along the a or c axis may result in a spin-flop-like transition. In general, the periodicity of the magnetic structure is expected to change in this transition.

To investigate the effects of a magnetic field, we have performed elastic neutron diffraction scans in the vicinity of the (0.5, 1.5, 0.5) reciprocal-lattice position in sample 2. The horizontal scattering plane coincided with the $(h, 3k, k)$ zone, and the field was perpendicular to the scattering plane. In this geometry, the magnetic field has no a-axis component, and the angle between the field and the c axis is $22°$.

The diffraction scans taken at $T = 10$ K in various magnetic fields are shown in Fig. 8. As may be seen in Fig. 8, application of a magnetic field results in a substantial reduction of the incommensurability of the magnetic structure. That is, the diffraction peaks move closer to the "commensurate" $h = 0.5$ position. However, even in a field of 8 T, the magnetic structure in the a direction is still incommensurate. An unexpected result is the measurable broadening of the diffraction peaks with the application of a magnetic field (compare scans at zero field and at $H = 5$ T in Fig. 8). This broadening indicates that the long-range magnetic order characteristic of the zero-field magnetic structure is destroyed at high magnetic fields.
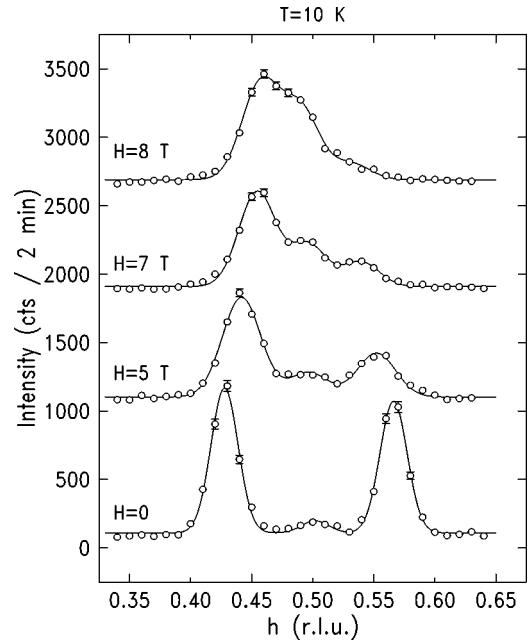

FIG. 8. Neutron-diffraction scans along the $(h, 1.5, 0.5)$ direction at $T = 10$ K in various magnetic fields. Each scan is shifted along the y axis by a constant offset value. The solid lines are results of the fits as described in the text.

The data of Fig. 8 have been fitted to the sum of three Gaussian peaks. The results of the fits are shown as solid lines in Fig. 8. Figure 9 shows the magnetic-field dependence of the intensities of all the three peaks, the separation between the incommensurate peaks, and the full peak width at $T = 10$ K. In agreement with the susceptibility data for the magnetic field parallel to the c axis, the transition begins at $H \sim 3$ T and is not complete at $H = 5$ T. In fact, it is evidently not complete even at $H = 8$ T, as the data of Fig. 9 show. The redistribution of the scattered intensity between the different peaks in Fig. 8 reflects the field-induced changes in the magnetic structure; a more extensive diffraction experiment is required to determine the high-field magnetic structure. To determine the high-field correlation length, the data have been fitted to an intrinsic 3D Lorentzian cross section convoluted with the experimental resolution function. For the correlation length along the a axis, we obtain $\xi_a = 250$ Å ± 80 Å. The transverse resolution is too coarse to allow us to determine the correlation length in the transverse direction $(0.5, 3k, k)$.

The temperature dependences of the peak intensities, the separation between the incommensurate peaks, and the full peak width at $H = 6.9$ T are shown in Fig. 10. The correlation length at this field is always finite, and no well defined phase transition is observed. Note that at high temperatures the period of the incommensurate spin modulation reverts back to the value characteristic of the zero-field magnetic structure.

The unexpected result of our experiment is the finite correlation length of the high-field state. The domain size in this state (200–300 Å) is certainly large. However, as the data of Fig. 10 show, there is no well defined phase transition as a function of temperature in the high-field state. This type of
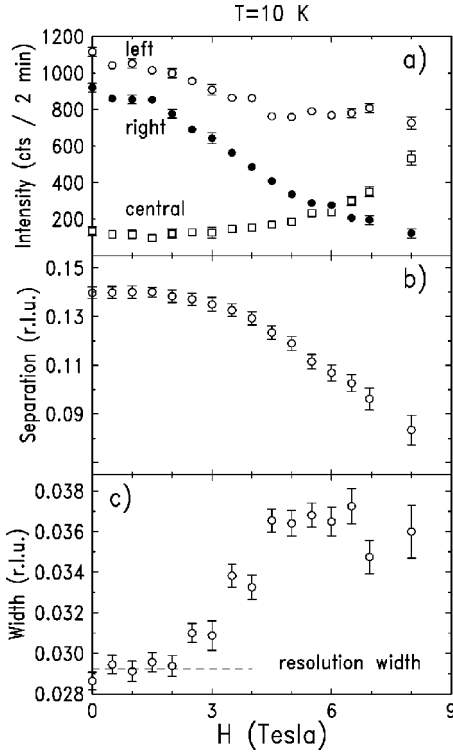
FIG. 9. Magnetic-field dependence of the peak intensity (a), the separation between the incommensurate peaks (b), and the full peak width (c) at $T=10$ K. The data were taken in the vicinity of the (0.5, 1.5, 0.5) position, as shown in Fig. 8. The scanning direction was (h, 1.5, 0.5). The ''left,'' ''central,'' and ''right'' keys in (a) refer to the lower, intermediate (commensurate), and higher h peaks in Fig. 8.
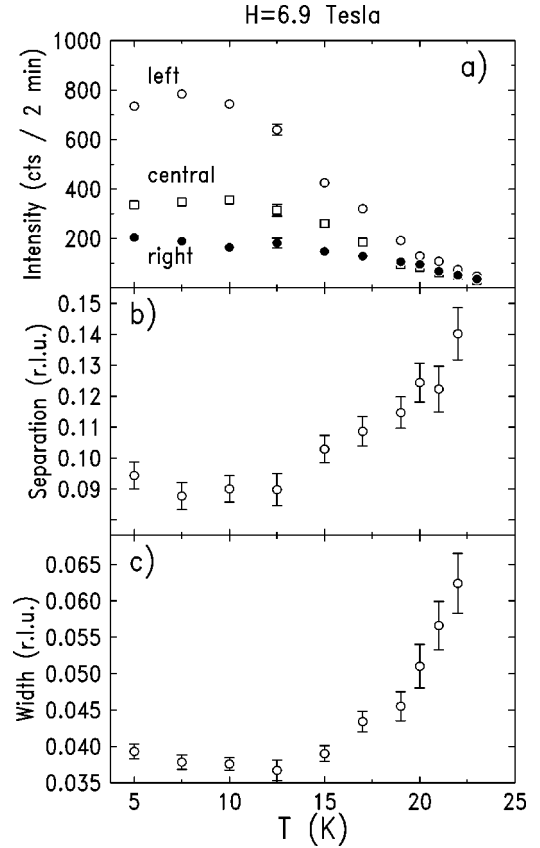

FIG. 10. Temperature dependence of the peak intensity (a), the separation between the incommensurate peaks (b), and the full peak width (c) at $H=6.9$ T. The scattering geometry and the keys in (a) are the same as in Fig. 9.

behavior is often found in magnetic systems with quenched disorder such as, for example, the doped spin-Peierls compound $CuGeO_3$ or random-field Ising materials.[31,32] In some of these materials, the application of a magnetic field also results in the destruction of long-range order.[31] Therefore one possible explanation of the finite correlation length in the magnetic field is that it is due to impurity effects. The magnetic long-range order can be destroyed, for example, by random fields that arise due to the presence of impurities in an antiferromagnetic system in which the applied field has a component along the direction of the spins.[33,32] In our samples, the loss of long-range order coincides with a transition from a state with magnetic periodicity which is a rational fraction of the unit-cell length (7/3) to a series of intermediate states which exhibit the periodicity that is not such a rational fraction in the range of the magnetic fields used in our experiment. This gives an additional argument in favor of the important role of impurities because impurity effects are, in general, more pronounced in systems with continuous symmetry than in systems exhibiting periodic ''locked'' structures. As mentioned above, the nonzero Curie constants found in our samples as well as our powder-diffraction measurements suggest that either impurities or structural disorder might indeed be present in our samples.

While long-range order is found in the zero-field state, the

very existence of magnetic ordering in $CaCu_2O_3$ may also be due to the presence of structural imperfections because the ground state of low-dimensional systems is extremely sensitive to even a small amount of disorder[34,31]. It is well known, for example, that while pure $SrCu_2O_3$ stays in the spin liquid state down to the lowest temperatures, substitution of just a few percent of copper ions with zinc induces low-temperature magnetic ordering.[34] At this stage, the precise control of the chemical composition of our samples has not yet been achieved. It is evident, however, that disorder can play a very important role in this material, and the synthesis of single crystals with a controlled amount of disorder is highly desirable.

V. SUMMARY

In summary, we have carried out magnetic susceptibility and neutron-diffraction studies of the $S=\frac{1}{2}$ quasi-one-dimensional magnet $CaCu_2O_3$. Above $T=50$ K, the magnetic susceptibility of this material is in good agreement with the results of Monte Carlo calculations for a model consisting of 1D spin-$\frac{1}{2}$ Heisenberg chains broken into weakly interacting segments of finite size with $J_{\parallel}=2000\pm300$ K, plus an additional small Curie term due to extrinsic impurities. $CaCu_2O_3$ undergoes a phase transition to an incommensurate magnetically ordered state at $T_N\sim25$ K. The ordering wave

vector is $[0.429(5), \frac{1}{2}, \frac{1}{2}]$. The magnetic structure is incommensurate (or high oder commensurate) in the direction of the frustrated interchain interaction. Weak commensurate magnetic Bragg peaks with the reduced wave vector $(\frac{1}{2}, \frac{1}{2}, \frac{1}{2})$ are also observed below T_N. The experimental data are consistent with a spiral (or possibly conical) magnetic structure with spins rotating in the ac crystallographic plane. The low-temperature magnitude of the ordered magnetic moment determined using this model magnetic structure is $0.2 \pm 0.07 \mu_B$.

Application of a magnetic field induces a metamagnetic transition at which the incommensurability of the magnetic structure is substantially reduced. Surprisingly, only a short-range order is found in the high-field state. The correlation length of the high-field state (200–300 Å) is, however, relatively large. The finite correlation length found in this state presumably results from impurity effects, as discussed in Sec. IV.

In brief, $CaCu_2O_3$ is an experimental quasi-1D magnetic system that provides an interesting opportunity to study the effects of quantum magnetism, magnetic frustration, and anisotropic magnetic interactions, and in which impurity effects can play a significant role. These subjects are currently attracting an intense attention of condensed-matter physicists. Further experimental and theoretical investigation of $CaCu_2O_3$ is therefore of considerable interest.

ACKNOWLEDGMENTS

---

*Present address: Dept. of Physics. and Astronomy, Rutgers University, Piscataway, NJ 08854.

†Present address: Dept. of Physics, University of Toronto, Toronto, Ontario, Canada M5S1A7.

[1] H. A. Bethe, Z. Phys. **71**, 205 (1931); A. Luther and I. Peschel, Phys. Rev. B **9**, 2911 (1974).

[2] S. Chakravarty, B. I. Halperin, and D. R. Nelson, Phys. Rev. B **39**, 2344 (1989).

[3] E. Dagotto and T. M. Rice, Science **271**, 618 (1996), and references therein.

[4] Z. Hiroi, M. Azuma, M. Takano, and Y. Bando, J. Solid State Chem. **95**, 230 (1991).

[5] J. B. Goodenough, Phys. Rev. **100**, 564 (1955); J. Kanamori, J. Phys. Chem. Solids **10**, 87 (1959); P. W. Anderson, Solid State Phys. **14**, 99 (1963).

[6] Von C. L. Teske and H. Müller-Buschbaum, Z. Anorg. Allg. Chem. **370**, 134 (1969).

[7] R. S. Roth, C. J. Rawn, J. J. Ritter, and B. P. Burton, J. Am. Ceram. Soc. **72**, 1545 (1989); R. O. Suzuki, P. Bohac, and L. J. Gauckler, *ibid.* **77**, 41 (1994); D. Risold, B. Hallstedt, and L. J. Gauckler, *ibid.* **78**, 2655 (1995).

[8] A. C. Larson and R. B. Von Dreele, Los Alamos National Laboratory, Report No. LAUR-86-748 (unpublished).

[9] A. R. King and H. Rohrer, Phys. Rev. B **19**, 5864 (1979).

[10] N. Motoyama, H. Eisaki, and S. Uchida, Phys. Rev. Lett. **76**, 3212 (1996).

[11] D. C. Johnston, Phys. Rev. B **54**, 13 009 (1996).

[12] For a review, see M. Imada, A. Fujimori, and Y. Tokura, Rev. Mod. Phys. **70**, 1039 (1998).

[13] M. Azuma, Z. Hiroi, M. Takano, K. Ishida, and Y. Kitaoka, Phys. Rev. Lett. **73**, 3463 (1994).

[14] Y. Mizuno, T. Tohyama, S. Maekawa, T. Osafune, N. Motoyama, H. Eisaki, and S. Uchida, Phys. Rev. B **57**, 5326 (1998).

[15] Monte Carlo calculations carried out for the values of $J_\perp / J_\parallel$ as high as 0.2 confirm this statement.

[16] M. Takahashi, Prog. Theor. Phys. **46**, 401 (1971); M. Takahashi and M. Suzuki, *ibid.* **48**, 2187 (1972); T. Koma, *ibid.* **81**, 783 (1988); M. Gaudin, Phys. Rev. Lett. **26**, 1301 (1971); S. Eggert, I. Affleck, and M. Takahashi, *ibid.* **73**, 332 (1994).

[17] P. W. Wood, *Magnetochemistry* (Interscience Publishers, New York, 1956).

[18] For a review, see H. G. Evertz, in *Numerical Methods for Lattice Quantum Many-Body Problems*, edited by D. J. Scalapino (Perseus Books, 1999).

[19] Y. J. Kim, M. Greven, U.-J. Wiese, and R. J. Birgeneau, Eur. Phys. J. B **4**, 291 (1998).

[20] I. E. Dzyaloshinsky, J. Phys. Chem. Solids **4**, 241 (1958).

[21] T. Thio, T. R. Thurston, N. W. Preyer, P. J. Picone, M. A. Kastner, H. P. Jenssen, D. R. Gabbe, C. Y. Chen, R. J. Birgeneau, and A. Aharony, Phys. Rev. B **38**, 905 (1988).

[22] T. Moriya, in *Magnetism*, edited by G. T. Rado and H. Suhl (Academic Press, New York, 1963).

[23] M. Greven and R. J. Birgeneau, Phys. Rev. Lett. **81**, 1945 (1998).

[24] See, e.g., S. Tornow, O. Entin-Wohlman, and A. Aharony, Phys. Rev. B **60**, 10 206 (1999), and references therein.

[25] F. C. Chou, A. Aharony, R. J. Birgeneau, O. Entin-Wohlman, M. Greven, A. B. Harris, M. A. Kastner, Y. J. Kim, D. S. Kleinberg, Y. S. Lee, and Q. Zhu, Phys. Rev. Lett. **78**, 535 (1997).

[26] A. Aharony, O. Entin-Wohlman, and A. B. Harris (unpublished).

[27] These interactions may also play an important role in the 1D magnet $La_6Ca_8Cu_{24}O_{41}$ which shows similar incommensurate magnetic ordering [M. Matsuda, K. Katsumata, T. Yokoo, S. M. Shapiro, and G. Shirane, Phys. Rev. B **54**, R15 626 (1996)].

[28] J. A. Riera and S. D. Dalosto, cond-mat/0008427 (unpublished).

[29] S. W. Lovesey, *Theory of Neutron Scattering from Condensed Matter* (Oxford University Press, New York, 1984).

[30] S. Shamoto, M. Sato, J. M. Tranquada, B. J. Sternlieb, and G. Shirane, Phys. Rev. B **48**, 13 817 (1993).

[31] V. Kiryukhin, B. Keimer, J. P. Hill, S. M. Coad, and D. McK. Paul, Phys. Rev. B **54**, 7269 (1996); Y. J. Wang, V. Kiryukhin, R. J. Birgeneau, T. Masuda, I. Tsukada, and K. Uchinokura, Phys. Rev. Lett. **83**, 1676 (1999).

[32] Q. J. Harris, Q. Feng, Y. S. Lee, Y.-J. Kim, R. J. Birgeneau, and A. Ito, Z. Phys. B: Condens. Matter **102**, 163 (1997); R. J. Birgeneau, J. Magn. Magn. Mater. **177-181**, 1 (1998).

[33] S. Fishman and A. Aharony, J. Phys. C **12**, L729 (1979).

[34] M. Azuma, Y. Fujishiro, M. Takano, M. Nohara, and H. Takagi, Phys. Rev. B **55**, R8658 (1997).